Mechanical Response of Variable and Constant-Stiffness Cylindrical Shells for Launcher Structures

Labans, Edgars; Bisagni, Chiara

Publication date
2018

Document Version
Accepted author manuscript

Published in
ECSSMET 2018: 15th European Conference on Spacecraft Structures

Citation (APA)
Labans, E., & Bisagni, C. (2018). Mechanical Response of Variable and Constant-Stiffness Cylindrical Shells for Launcher Structures. In *ECSSMET 2018: 15th European Conference on Spacecraft Structures: 2018, Noordwijk, Netherlands*

MECHANICAL RESPONSE OF VARIABLE AND CONSTANT-STIFFNESS CYLINDRICAL SHELLS FOR LAUNCHER STRUCTURES

Edgars Labans [(1)], Chiara Bisagni [(1)]

[(1)] *Delft University of Technology, Faculty of Aerospace Engineering, Kluyverweg 1, 2629 HS, Delft, The Netherlands, Email: e.labans@tudelft.nl, c.bisagni@tudelft.nl*

ABSTRACT

The ability to steer the carbon fibre tape, varying the tow angle can open new designs of cylindrical shells – the main structural component of the space launcher vehicles. This research presents experimental and numerical investigation of two carbon-epoxy cylindrical shells – a cylinder with conventional layup made of unidirectional prepreg and a variable-stiffness cylinder manufactured by applying advanced fibre placement technology. The shells were tested in compression until buckling, measuring load-shortening and capturing the buckling shape by digital image correlation systems. For the purpose of modelling the variable-stiffness cylinder, a simplified stiffness approximation approach was applied. The obtained load-shortening curves and buckling shapes demonstrated good correlation with non-linear numerical models. The results of the investigation contributes to the understanding the phenomenon of buckling of variable-stiffness cylindrical shells, and the influence of initial geometric imperfections and thickness variations.

1. INTRODUCTION

Thin-walled cylindrical shells are one of the main components of space launcher vehicles. To reduce weight several latest generation launcher vehicles like ARIANE 5 and VEGA have already implemented fibre based composite parts. The most recent ELECTRON rocket by ROCKETLAB relies heavily on the use of composites for outer shell cover and fuel tanks. Considering that buckling and stiffness are one of the main design characteristics of the launcher structures, variable-stiffness laminates could be successfully applied to improve them. One of the most convenient ways of manufacturing variable-stiffness structure is Advanced Fibre Placement (AFP) that allows to spatially change direction of the tow within a single composite layer. In this way, fibres can be placed in a wide variety of angles even changing tow orientation within a ply, leading to variable-stiffness laminates.

AFP machines are widely used in the industry to manufacture space structures since their development in the late 1980s [1] but only recently they were adjusted for curvilinear tow-placement. Initially, benefits of curvilinear fibres were reported by numerical and experimental studies on small-scale, flat variable-stiffness plates [2-5]. They demonstrated that substantial structural improvements in strength, stiffness and buckling load could be reached applying curved fibres and overlaps. The recent progress on design, optimisation and manufacturing of the variable-stiffness composites is summarized in review papers [6-7].

Whereas a lot of studies were conducted on a small scale flat specimens, only a few consider cylindrical shells. Nonetheless, constant-stiffness composite shells were investigated for decades, resulting in numerous experimental and numerical studies [8-11].

The buckling of the variable-stiffness cylinders in compression is described in several experimental works. For example, Wu published a paper on design, manufacturing and testing of two variable-stiffness Carbon Fibre Reinforced Plastic (CFRP) cylinders [12]. One of the cylinders was manufactured allowing overlaps, while a second one was made without overlaps to maintain constant thickness. Subsequent research is done with the same cylinders to assess the influence of large cut-outs [13].

The research on variable-stiffness cylinders is mostly based on numerical modelling [14-15]. The main results indicate that the buckling load of the variable-stiffness cylinders can be increased at least by 15%, comparing to the optimized constant-stiffness cylinder.

The aim of the current study is to obtain experimental data on the buckling behaviour of the variable-stiffness cylinders and to apply the simplified modelling approach for prediction of the stiffness and the buckling load of these structures.

2. CYLINDERS

The investigated cylinders were made by the Dutch National Aerospace Laboratory (NLR). The specimens have an inner diameter of 600 mm and a length of 790 mm. A photo of the cylinders is reported in Figure 1. Both cylinders are composed of 8 layers of AS4/8552 CFRP prepreg with the average thickness of 0.181 mm. After applying the lay-up on the steel mandrel with automated robot arm, cylinders were placed in autoclave for final curing.

The constant-stiffness cylinder has $[\pm 45/\ 0/\ 90]_s$ lay-up, while the variable-stiffness cylinder has the lay-up of $[\pm 45/\ \pm\varphi(x)]_s$, where $\pm\varphi(x)$ is a steered ply with constant course width. Stiffness of the shell varies along the vertical axis. The fibre angle at the top and the bottom of the cylinder is 60^0 and in the middle it is 15^0. Both cylinders have an end-potting made of epoxy resin and chopped glass fibres to be able to apply the load on the structure. Outer thickness of the potting is equal to 25 mm and inner thickness is equal to 15 mm. The potting covers 40 mm of the cylinder height at each end.

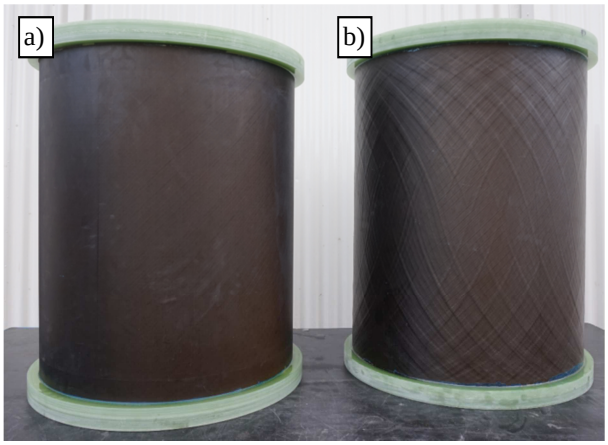

Figure 1. The cylinders with end-potting: a) the constant-stiffness cylinder; b) the variable-stiffness cylinder

3. GEOMETRIC IMPERFECTIONS

Geometrical imperfections of the cylinders were measured before the compression tests. Fine speckle pattern was applied on the surface of the cylinders to provide tracking points for the Digital Image Correlation (DIC) system. The average speckle dot size was 3 mm with filling density of 20%. The test set-up for the surface imperfection scan using VIC3D [16] DIC system is shown in Figure 2. The surface was measured from four sides, capturing approximately 130^0 of the cylinder area in one shot. After each shot the cylinder was turned by 90^0. Final array of the data points was combined in VIC 3D software to obtain the whole 3D shape of the cylinder.

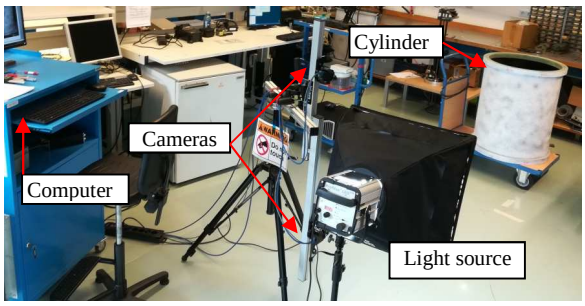

Figure 2. Test set-up of DIC for measuring of the geometric imperfections

Post-processing of the imperfection data was performed in Matlab. The best-fit radius of the cylinder was found and the measured geometric imperfections were characterized as deviation from the radius of the perfect cylinder. The wrapped surfaces of the cylinders with imperfection colour plots are given in Figure 3. Positive values on the colour bar indicate that imperfections are larger than the perfect radius and negative values that they are smaller. It is possible to note that the constant-stiffness cylinder in Figure 3.a is ovalized along the whole vertical axis and imperfection values reach ±1 mm.

Imperfection plot of the variable-stiffness cylinder in Figure 3.b has sufficient resolution to distinguish tows of overlapped fibres. It can be also seen that the global out-of-plane imperfections exceed the local imperfections caused by fibre overlaps. The cylinder is ovalized in the lower part with maximal outer imperfection values of 1.5 mm and bent inwards in two wide areas in the middle with imperfection values reaching -1 mm.

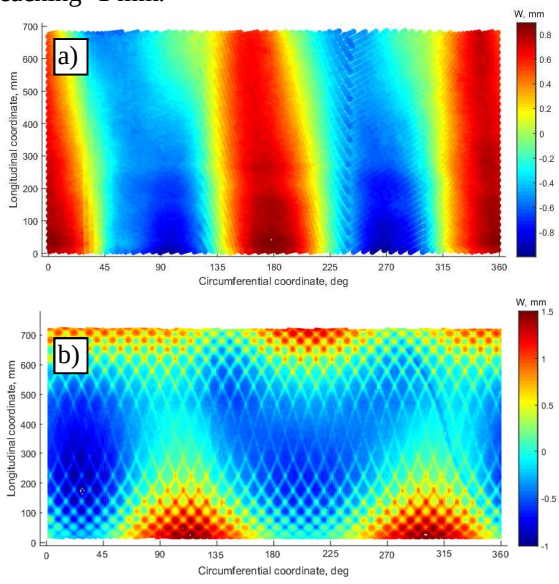

Figure 3. Geometric imperfections plots from DIC system: a) the constant-stiffness cylinder; b) the variable-stiffness cylinder

4. TEST SET-UP

The compression tests were performed using a MTS 3500 servo-hydraulic test machine shown in Figure 4. The cylinders were placed on a steel base plate and loaded by hydraulic actuator moving the upper plate by constant velocity equal to 0.25 mm/min.

Figure 4. MTS 3500 kN servo-hydraulic test machine: a) front view; b) side view

The uniform loading conditions were reached by adjusting self-levelling upper plate at the low load level. Displacements were measured by two LVDT displacement sensors on both sides of the specimen, as shown in Figure 4.b. The analog signals from the LVDTs were synchronized with the load and time

readings from the controlling computer.
Out-of-plane displacements were recorded using two VIC 3D DIC systems at the frequency of 1 Hz. Two systems covered front and rear side of each cylinder. Each DIC system was able to measure approximately 150^0 of the cylinder surface.
After the buckling of the cylinder, the test was manually terminated to prevent damage. The loading plate was slowly returned to the initial position with vertical velocity of 1 mm/min. The sequence of the DIC images were then post-processed to obtain the out-of-plane displacement plots.

5. NUMERICAL MODEL

Numerical analysis of the cylinders was performed in Abaqus [17]. The mesh of the cylinder, depicted in Figure 5, is based on S4R shell elements for the carbon fibre composite wall and C3D8R solid elements for the end-potting. A mesh step of 10 mm was chosen after performing mesh sensitivity study. The material properties of the AS4/8552 carbon fibre tape can be found in [18], whereas the mechanical properties of the end-potting were assumed as isotropic with the modulus of elasticity of 4.5 GPa and Poisson`s ratio of 0.3.
The boundary conditions were set to rigidly link the nodes on the edges of the cylinder to the central reference nodes as shown in Figure 5. Only vertical movement of the upper nodes was allowed.
The initial geometrical imperfections obtained by DIC system were integrated in the numerical model. The imperfection shapes magnified 50 times are shown in Figure 6.

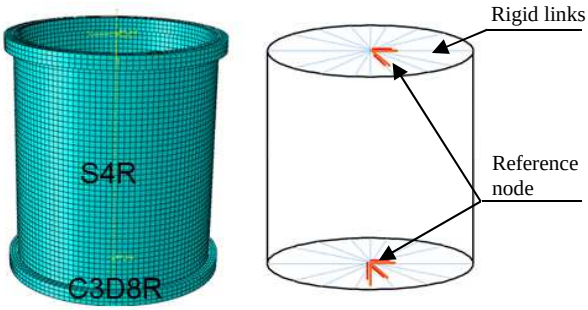

Figure 5. Mesh and boundary conditions in the numerical model

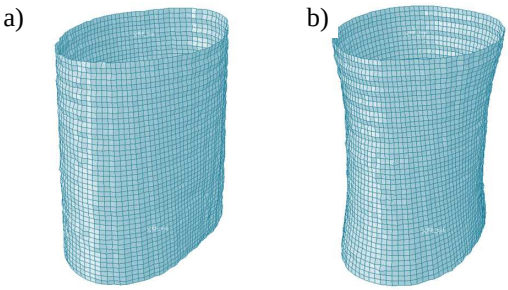

Figure 6. Magnified imperfection shapes (x50): a) the constant-stiffness cylinder; b) the variable-stiffness cylinder

A simplified approach was used to introduce stiffness variation of the laminate in the numerical model. The area of the cylinder was divided in separate sections along the height. Then, a constant layup and ply number was assigning for each of the section as shown in Figure 7. In addition, graphical representation of the laminate thickness along the height of the cylinder is given.
The fibre angle of each cylinder section was determined as the average value between the angle at the upper and the lower edge of the section. Additional steered plies were added for the end sections to compensate the effect of the overlaps. Three different approximations were investigated, starting from a coarse model with two distinct sections to a finer model with five sections.

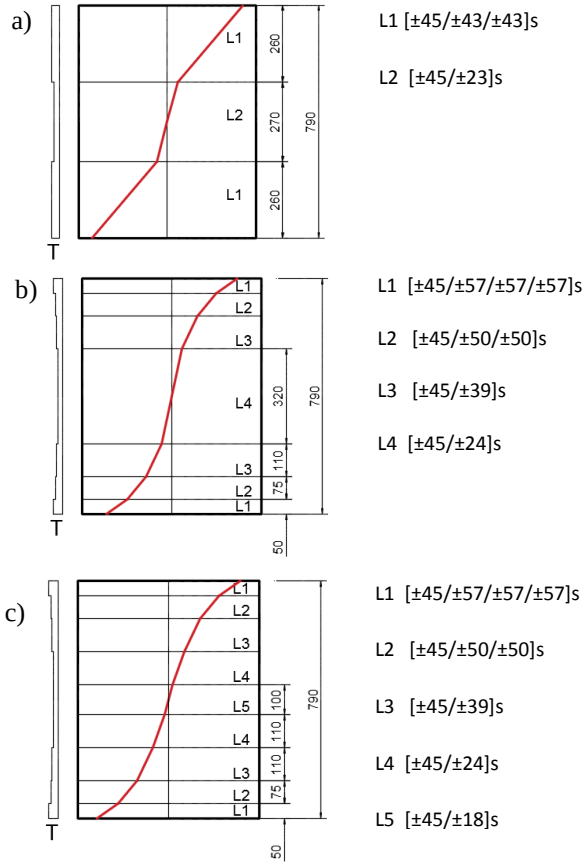

Figure 7. Approximated models of the variable-stiffness cylinder: a) two sections; b) four sections; c) five sections

6. RESULTS

During the tests, a linear load-shortening response was recorded for both cylinders followed by a sharp load-drop at the buckling. Both cylinders presented a pattern of two-row buckles. The tests also demonstrated good repeatability leading to the same buckling load and buckling shape after several consequent loadings and unloading cycles.
Obtained buckling load of the constant-stiffness cylinder was 303 kN and buckling load for variable-stiffness cylinder was 208 kN. As expected, the buckling load and the stiffness of the variable-stiffness

cylinder was lower due to the non-optimized lay-up.
The numerical results for the constant-stiffness cylinder, shown in Figure 8, have a good correlation to the experimental load-shortening curve, although the numerical results are in average 5% higher in terms of stiffness and buckling load.

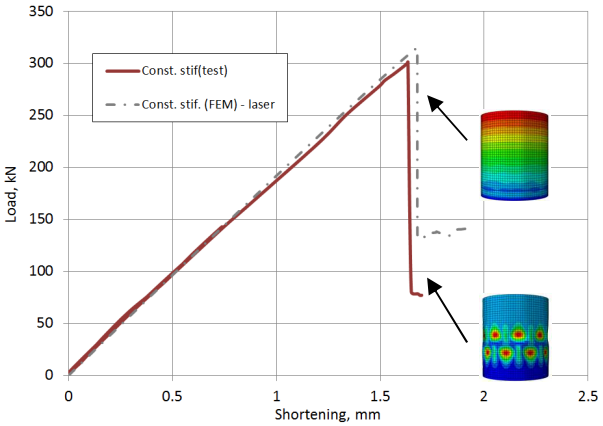

Figure 8. Load–shortening curves of the constant-stiffness cylinder

The experimental and numerical load-shortening curves of the variable-stiffness cylinder are reported in Figure 9. Three variations of the simplified numerical model are shown in the same figure, marked with dashed lines.

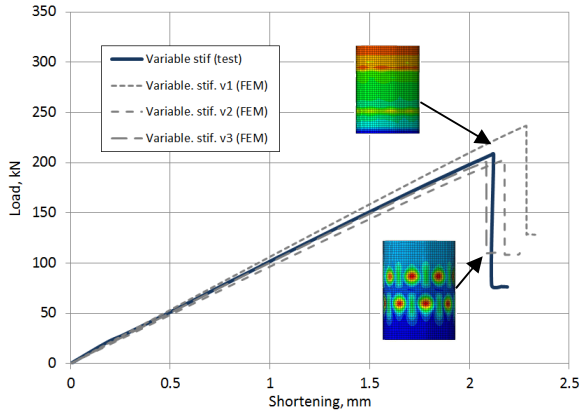

Figure 9. Load–shortening curves of the variable-stiffness cylinders

It can be seen that an increase of the number of the sections in the simplified numerical models improve the accuracy of the numerical prediction. Additional sections in the third model provides slight increase in the stiffness, comparing to the curve of the second model.
The experimental buckling shapes of the cylinders are shown in Figure 10. Both cylinders have uniform buckle pattern in two rows. The variable-stiffness cylinder was tested later, therefore it has an improved speckle pattern for easier visual recognition of the shape. The same buckling shapes, post-processed by the DIC system, are shown in Figure 11. Both cylinders have similar colour patterns and also similar amplitudes of the out-of-plane displacements.
The out-of-plane values of the numerical models, shown in Figure 12, have a close match to the experimental results when the buckling shape and also displacement values are compared. The colour bar in DIC software and in numerical model shows displacement values in Cartesian coordinate system, therefore the buckles at the edges of the covered area seem shallower.

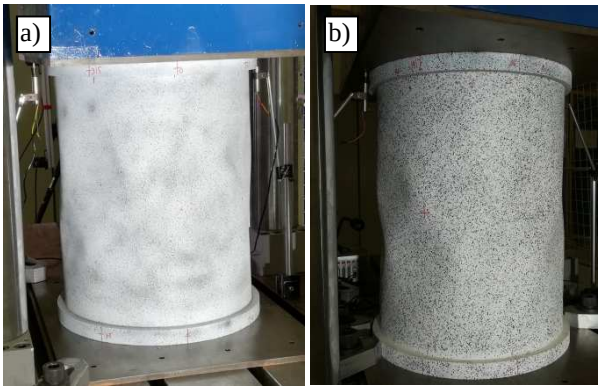

Figure 10. Buckling shape: a)the constant-stiffness cylinder; b) the variable-stiffness cylinder

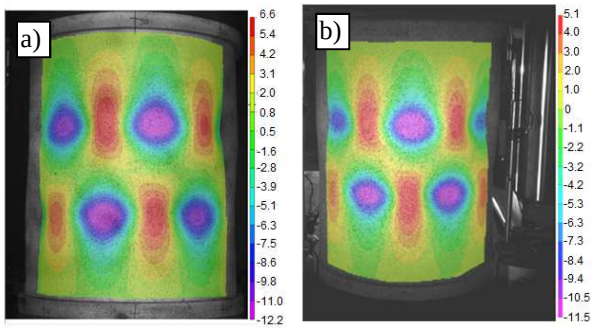

Figure 11. Buckling shapes acquired by DIC system: a) the constant-stiffness cylinder; b) the variable-stiffness cylinder

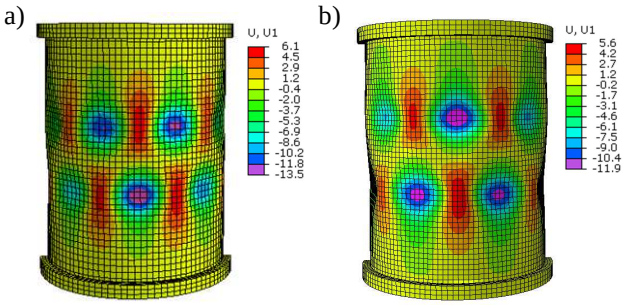

Figure 12. Buckling shapes obtained by the numerical analysis: a) the constant-stiffness cylinder; b) the variable-stiffness cylinder

The maximum experimental outward displacement of the constant-stiffness cylinder is 6.6 mm and inward displacement is -12.2 mm. The variable-stiffness cylinder shows slightly lower displacements of 5.1 mm and -11.5 mm, respectively. Numerical models have approximately 10% higher maximum inwards and outwards displacement values as well as smaller distance between upper and lower row of buckles.

7. CONCLUSIONS

This study analysed two types of CFRP cylinders in compression: a constant-stiffness and a variable-stiffness cylinder. The tests were conducted using a hydraulic test rig with displacement driven control, measuring the displacements with LVDTs and two DIC systems. Prior to the tests, initial geometric imperfections were measured.

Both cylinders presented a similar behaviour traits like elastic load-shortening curves, rapid loss of load bearing capacity at buckling and regular buckling shape. In addition, repeatability of the buckling load was reached for both cylinders.

The acquired experimental results provide information about the load-shortening curves and out-of-plane displacement pattern. Considering that experimental data on variable-stiffness cylinders are scarce, the research provide useful information for further model validations and implementation of the variable-stiffness laminates in launcher structures.

A simplified numerical modelling approach for the variable-stiffness cylinder was efficient to predict stiffness and buckling load for the shells with variable fibre angles. Hence output of the model is directly related to the number of sections used for the stiffness approximation.

The future studies will be directed towards vibration analysis and optimisation of the variable-stiffness composite cylinders.

8. REFERENCES

1. Kisch, RA. (2006). Automated Fiber Placement Historical Perspective. *Proceedings of International SAMPE Symposium and Exhibition*. Long Beach, United States, 1-65.

2. Hyer, M. & Lee, H., (1991). The Use of Curvilinear-Fiber Format to Improve Buckling Resistance of Composite Plates with Central Holes. *Compos. Struct*, **18**(3), 239–261.

3. Tatting, B.F. & Gurdal, Z. (2003). Automated Finite Element Analysis of Elastically-Tailored Plates. *NASA/CR-2003-212679*, December 2003.

4. van Campen, J., Kassapoglou, C., & Gürdal, Z. (2012). Generating Realistic Laminate Fiber Angle Distributions for Optimal Variable-Stiffness Laminates," *Compos. Part B Eng*. **43**(2), 354–360.

5. Peeters, D. & Abdalla, M. (2017). Design Guidelines in Nonconventional Composite Laminate Optimization. *J. Aircraft*. **54**(4), 1454-1464.

6. Sabido, A., Bahamonde, L., Harik, R. & Tooren, M.J.L. (2017). Maturity Assessment of The Laminate Variable-Stiffness Design Process. *Compos Struct*. **160**(1), 804 -812.

7. Lozano, G., Tiwari, A., Turner, C. & Astwood S. (2016). A Review on Design for Manufacture of Variable-Stiffness Composite Laminates. *J. Eng. Manuf.* **230**(6), 981-992.

8. ECSS-E-HB-32-24A – Buckling of structures, Noordwijk, The Netherlands, 2010.

9. Bisagni, C. (2000). Numerical Analysis and Experimental Correlation of Composite Shell Buckling and Post-Buckling. *Comp. Part B*, **31**(8), 655-667.

10. Bisagni, C. (2015). Composite Cylindrical Shells under Static and Dynamic Axial Loading: an Experimental Campaign. *Prog. Aerosp. Sci*, **78**(1), 107-115.

11. Kalnins, K., Arbelo, M.A., Ozolins, O., Skukis, E., Castro, S.G.P. & Degenhardt, R. (2015). Experimental Nondestructive Test for Estimation of Buckling Load on Unstiffened Cylindrical Shells Using Vibration Correlation Technique. *Shock. Vib*. **172**(1), 1023-1030.

12. Wu, K.C., Tatting, B.F., Smith, B.H., Stevens, R.S., Occhipinti, G.P., Swift, J.B., Achary, D.C., & Thornburgh, R.P. (2009). Design and Manufacturing of Tow-Steered Composite Shells using Fiber Placement. *Proceedings of the 50th AIAA/ASME/ASCE/AHS/ASC Structures, Structural Dynamics and Materials Conference*, CA, USA.

13. White, S.C., Weaver, P.M. & Wu, K.C. (2015). Post-Buckling Analyses of Variable-Stiffness Composite Cylinders in Axial Compression. *Compos. Struct*. **123**(1), 190-203.

14. Rouhi, M., Ghayoor, H., Hoa, S.V. & Hojjati, M. (2014). Effect of Structural Parameters on Design of Variable-Stiffness Composite Cylinders made by Fiber Steering. *Compos Struct.* **118**(1), 472-481.

15. Sun, M. & Hyer, M.W. (2008). Use of Material Tailoring to Improve Buckling Capacity of Elliptical Composite Cylinders. *AIAA J*, **46**(3), 770-782.

16. VIC-3D v7 (2016). Reference Manual, *Correlated Solutions*.

17. ABAQUS/Standard User's Manual (2017). Version 2017 ABAQUS. Inc. USA.

18. Hexcel Material Datasheet, 2016.